Diversity-Sensitive Generative Adversarial Network for Terrain Mapping Under Limited Human Intervention

Jianqiang Li, Zhuangzhuang Chen, Jie Chen, and Qiuzhen Lin

***Abstract*—In a collaborative air–ground robotic system, the large-scale terrain mapping using aerial images is important for the ground robot to plan a globally optimal path. However, it is a challenging task in a novel and dynamic field without historical human supervision. To alleviate the reliance on human intervention, this article presents a novel framework that integrates active learning and generative adversarial networks (GANs) to effectively exploit small human-labeled data for terrain mapping. In order to model the diverse terrain patterns, this article designs two novel diversity-sensitive GAN models which can capture fine-grained terrain classes among aerial image patches. The proposed approaches are tested in two real-world scenarios using our collaborative air–ground robotic platform. The empirical results show that our methods can outperform their counterparts in the predictive accuracy of terrain classification, visual quality of terrain mapping, and average length of the planned ground path. In practice, the proposed terrain mapping framework is especially valuable when the budget in time or labor cost is very limited.**

***Index Terms*—Active learning (AL), generative adversarial network (GAN), multiagent system.**

I. Introduction

RECENTLY, with the advance of unmanned aerial vehicle (UAV), unmanned ground vehicle (UGV), and information and communication technologies, collaborative air–ground robotic systems show potential for success in extensive scenarios (e.g., traffic monitoring, overcrowd detection, environmental sensing, search and rescue, civil security, and merchandise delivery) in smart cities [1]–[3]. To fulfill those missions, ground path planning is one of the key functionalities to enable UGV to navigate the urban area [4]. However, it is a challenging task as UGVs often have to operate in GPS-denied (due to street canyon effect) and unknown urban fields. Due to the limited range of on-board perception on ground vehicles and the complex objects (e.g., obstacles, ground surface, and vegetation) scattered in the indoor/outdoor environment, a single UGV tends to plan a myopic path which could waste time, incur energy cost, or cause mission failure. Fortunately, in a collaborative air–ground robotic system, UGV can exploit auxiliary aerial images from UAV to obtain a larger view of the urban field [5]–[10]. Thus, it is important to effectively learn the terrain map from aerial images for the nonmyopic ground path planning.

Terrain mapping aims to understand semantic terrain class, traversability, and other physical properties given a region on terrain [11]–[15]. Traditionally, terrain classification is usually conducted using sensors on UGVs [12]–[14], [16], [17] to predict attributes of distant terrain. However, these approaches have limited capabilities in terrain mapping due to the short sensing range of sensors on the ground robots. Thus, it would be beneficial to exploit an aerial image to perform terrain classification in a large scale. Terrain classification using aerial images can be categorized into fully autonomous methods [10] and human-intervened approaches [17]–[19]. The former methods are based on image processing techniques that can build the terrain map without any human intervention. However, due to lack of supervision, they are poorly adaptable to dynamic environmental conditions (e.g., time-varying light conditions and different weathers). On the other hand, the latter methods exploit machine-learning techniques to achieve better mapping accuracy with certain human supervision; However, those models rely on a sufficiently large training set where each point has to be labeled by experienced domain experts. For instance, the semantic segmentation methods [7] have to assign a class (e.g., road, building, and tree) to each pixel of the training data by hand. The performance of the approaches relies on extensive pixel-level manual annotation which is costly in time/human labor, and hence impractical to be deployed in a novel field. In contrast, we assume only a limited human intervention in annotating a small number of examples and determining the traversability of terrain classes.

With only a small human-labeled training data, generative models can be exploited to enlarge the training data with generative examples. Generative adversarial network (GAN) [20] has emerged as an effective model for image generation. A typical GAN model consists of a generator and a discriminator that work adversarially to learn the true data distribution of a given dataset. Besides the success in image generation,

Manuscript received August 17, 2019; revised November 2, 2019; accepted December 9, 2019. This work was supported in part by the National Nature Science Foundation of China under Grant U1713212, Grant 61572330, Grant 61836005, and Grant 61702341, in part by the Natural Science Foundation of Guangdong Province-Outstanding Youth Program under Grant 2019B151502018, in part by the Technology Research Project of Shenzhen City under Grant JSGG20180507182904693, and in part by the Public Technology Platform of Shenzhen City under Grant GGFW2018021118145859. This article was recommended by Associate Editor L. Cheng. *(Corresponding author: Jie Chen.)*

The authors are with the College of Computer Science and Software Engineering, Shenzhen University, Shenzhen 518060, China (e-mail: chenjie@szu.edu.cn).

Color versions of one or more of the figures in this article are available online at http://ieeexplore.ieee.org.

Digital Object Identifier 10.1109/TCYB.2019.2962086

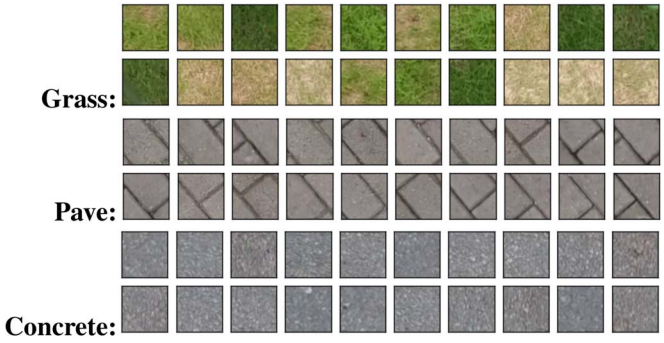

Fig. 1. Diverse image patches from different terrain classes.

GAN is exploited to enlarge the size of dataset for training classifiers [21], [22]. GAN models have been reported to be more effective than the traditional data augmentation techniques [23]–[26]. Existing GAN models can be broadly categorized into unconditional models [20], [23], [27] and conditional models [24], [26], [28], [29]. The unconditional GAN models have no control on modes in the generative data, thus not suitable for multiclass data. On the other hand, the conditional GAN (CGAN) models suffer from: 1) no consideration of hierarchical latent representation [28] and 2) requirement of a large amount of human-labeled training data [23].

To further improve the quality of generative examples from GAN, it is important to make the human labels more informative, especially, when the number of labels is extremely small. Active learning (AL) techniques have been exploited to work with various classifiers when labeled training data is small due to a limited budget in time or labor cost. The existing frameworks include: 1) AL coupled with support vector machine (SVM) [30]–[33] which uses probabilistic outputs of SVM classifier over different class labels to estimate uncertainty; 2) AL coupled with the Gaussian process (GP) model [34]–[38] which benefits from analytical quantification of the predictive uncertainty supported by the GP model; and 3) AL coupled with convolutional neural network (CNN) [39]–[41], which allows the framework to work with high-dimensional data and compute the uncertainty using the softmax layer of CNNs. To the best of our knowledge, there is very limited research on AL coupled with GAN models [42], [43]. In this article, the small training set is collected by using AL strategies [31], [41], [44] coupled with the terrain classifier to select those informative/uncertain examples for labeling.

Though GAN can be used to address insufficient training data issue, the quality of the generative examples could degenerate due to a poor modeling of diversity [23], [24], [26]. In our scenario of terrain mapping using aerial images, the image patches in different terrain classes (i.e., grass, pave, and concrete) consist of very diverse subclasses (see Fig. 1). In this article, the proposed approach can address the above issue in two aspects: 1) incorporating fine-grained diversity modeling of terrain classes into GAN and 2) coupling AL strategy with terrain classifier to improve the diversity of human labeled training data.

The contributions of this article are listed as follows.

TABLE I
USED NOTATIONS IN THIS ARTICLE

Notations	Description
$\mathbf{X}$	Matrix denoting an image patch
$\mathbf{z}$	Vector of noise variables
$\mathbf{c}$	Vector denoting coarse-grained representation
$\mathbf{s}$	Vector denoting fine-grained representation
p_{noise}	Noise distribution
p_{data}	Real data distribution
N	Number of terrain classes
$G(\mathbf{z};\theta_G)$	Generator of GAN model
$D(\mathbf{X};\theta_D)$	Discriminator of GAN model
$Q(\mathbf{c};\theta_Q)$	Approximation of $p(\mathbf{c} \mid \mathbf{X})$
$V(G,D)$	Objective function of GAN model
$\alpha(\mathbf{X};\theta_\alpha)$	Acquisition function for AL strategy
$\mathcal{X}_U$	A set of unlabelled patches
$\mathcal{X}_L$	A set of labeled image patches
$y_{\mathbf{X}}$	Label corresponding to $\mathbf{X}$
$\mathbb{H}[.]$	Entropy of a distribution
$\mathbb{E}[.]$	Expectation w.r.t. a distribution
$\mathbb{KL}[;]$	Kullback-Leibler Divergence between two distributions
$\mathbb{I}[;]$	Mutual information between two distributions
$\mathcal{M}$	CNN model
$\mathcal{G}$	GAN model

1) We present a novel framework that integrates GAN and AL strategy (Section II) for reducing the human intervention in terrain mapping using aerial images.
2) Two novel diversity-sensitive GAN models with different degrees of human intervention for incorporating fine-grained terrain classes (Section III) are proposed to improve the quality of the generative training data for terrain classifier.
3) A collaborative air–ground robotic system is implemented for testing the above proposed approaches (Section IV-A).
4) The experimental results show that our approach can achieve the best performance in accurate terrain mapping and be used to plan the shortest ground path (Section IV).

II. BACKGROUND

This section first describes the overall idea of terrain mapping in a collaborative air–ground robotic system. Then, we briefly explain the GAN models and AL strategies which can be exploited to address the terrain classification issue with small training data. To facilitate the readers, the important notations used in this article are summarized in Table. I.

A. Classic Terrain Mapping in Collaborative Air–Ground Robotic System

In a collaborative air–ground robotic system, the common workflow to build a terrain map using aerial images for ground path planning [5], [10], [16] consists of the following steps (see the parts of Fig. 2 which are connected by black lines).

First, the UAV performs visual perception to collect real-time aerial images that aim to cover a large part of the field using the on-board camera. Then, a set $\mathcal{X}_U$ of patches with unknown terrain classes can be formed by cropping the aerial images into small patches at certain fixed resolution.

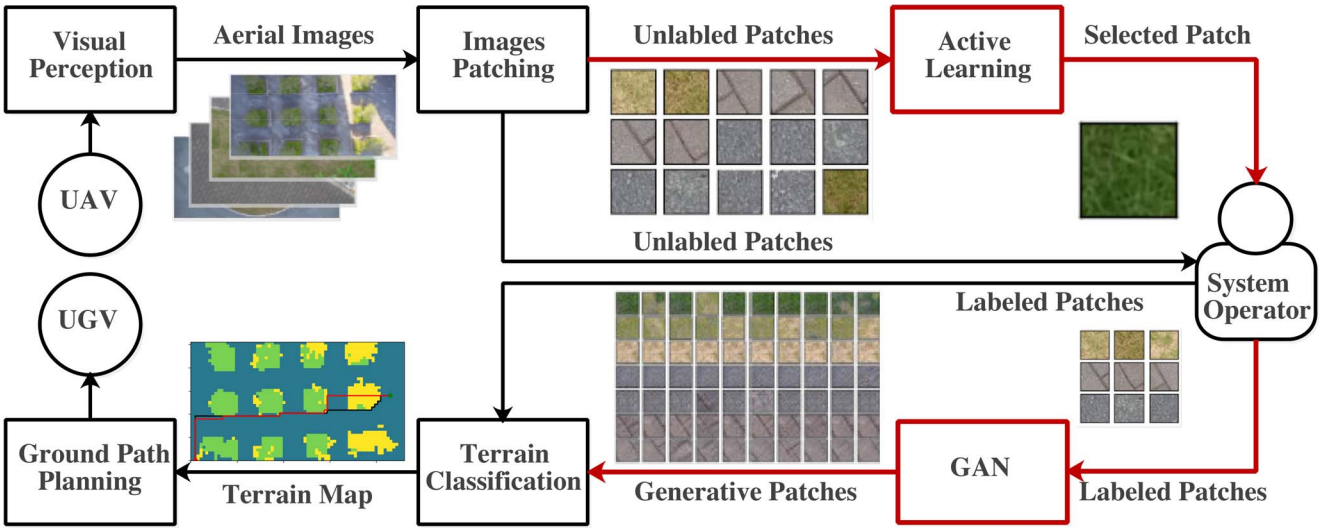

Fig. 2. New workflow of terrain mapping in the collaborative air–ground robotic system with limited human intervention.

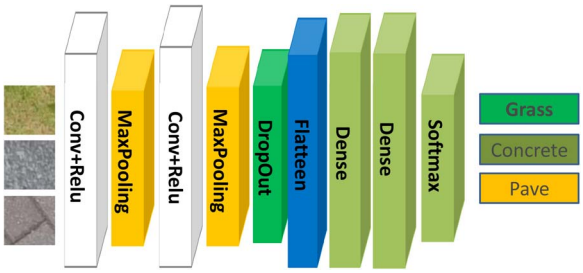

Fig. 3. Network structure of the CNN-based terrain classifier using aerial images.

Second, those unlabeled patches will be randomly selected from $\mathcal{X}_U$ to the system operators for annotating their terrain classes. An arbitrarily selected image patch $\mathbf{X} \in \mathcal{X}_U$ is labeled with $y_{\mathbf{X}}$ indicating the terrain class (e.g., grass, pave, and concrete) and put into a set $\mathcal{X}_L$, which contains all labeled patches.

Third, the labeled set $\mathcal{X}_L$ is used as the training data to learn a terrain classifier which is commonly chosen as CNN-based models. Existing work has successfully exploited the CNN model to estimate the terrain class in a gridded ground surface map [5]. Briefly, the CNN-based terrain classifier (shown in Fig. 3) is a cascade of Convolutional (conv), and rectified linear units (ReLU) layers, MaxPooling, Flatten and Dense layers. Such a network structure is reported to be successful in many recognition tasks [45].

Finally, the terrain classifier is exploited to build an online terrain map which is integrated with the UGV local map and path planning component to obtain a globally optimal path. Many research works [46]–[48] have been devoted to building a local map of the ground field with simultaneous localization and mapping (SLAM) algorithms running on UGV. For practitioners, the terrain map can easily be integrated with the local map of OpenSlam's Gmapping package[1] implemented in the robotic operating system.

[1]http://wiki.ros.org/gmapping/

In the above workflow, the accuracy of CNN-based terrain classifier relies on sufficient training data that require extensive annotations from experienced system operators. This hinders the system from deployment in a novel field as the human labor tends to be costly and limited. To address the issue caused by insufficient training data, this article proposed a new workflow (see Fig. 2) which incorporates two ideas from the machine-learning community to reduce human intervention: 1) GAN models are exploited to generate sufficient "fake" training samples that are as "real" as those in $\mathcal{X}_L$ and 2) AL strategies are exploited to improve the quality of the small training data $\mathcal{X}_L$ by choosing the most informative/uncertain image patches from unlabeled set $\mathcal{X}_U$ for labeling. We will explain these details in the following sections.

B. Active Learning-Enhanced Generative Adversarial Network

The original GAN [20] consists of two components: 1) a generator $G(\mathbf{z}; \theta_G)$ which can produce generative image patches as real as possible and 2) a discriminator $D(\mathbf{X}; \theta_D)$ which aims to differentiate the generative image patches from the real ones. The objective function of the original GAN is then defined as a two-player minmax game

$$\min_{\theta_G} \max_{\theta_D} V_{GAN}(G, D) = \mathbb{E}_{\mathbf{X} \sim p_{\text{data}}}\left[\log D(\mathbf{X})\right] + \mathbb{E}_{\mathbf{z} \sim p_{\text{noise}}}\left[\log(1 - D(G(\mathbf{z})))\right] \quad (1)$$

where p_{data} represents the real data distribution, p_{noise} is a noise variable, $G(\mathbf{z}; \theta_G)$ and $D(\mathbf{X}; \theta_D)$ are deep neural networks parametrized by θ_G and θ_D, respectively. θ_G is optimized such that $G(\mathbf{z}; \theta_G)$ can transform noise variables $\mathbf{z}$ into a generative sample $\mathbf{X}$ which has minimum probability of being identified as fake by $D(\mathbf{X}; \theta_D)$. On the other hand, θ_D is optimized such that the probability of correctly identifying an image patch $\mathbf{X}$ is maximized.

Though the GAN model can generate sufficient training data for CNN-based terrain classifier, the quality of the generative

data relies largely on a well-trained GAN model which again requires a sufficiently large number of human labeled patches. This is unfavorable in this article as human intervention is assumed to be limited. Intuitively, such issue can be alleviated if we only ask human to label those patches which can benefit most for training the GAN models. To achieve this goal, AL strategy coupled with CNN-based classifier [49] is designed to select more informative points from unlabeled set $\mathcal{X}_U$; Those selected points are then labeled by system operators. In the following, we describe how to incorporate the AL strategy into the proposed framework (see Fig. 2).

At the beginning, the labeled set $\mathcal{X}_L$ starts from empty and the aerial images are cropped into patches which are collected in the unlabeled set $\mathcal{X}_U$. Then, the active learning procedure aims to iteratively select the best patch from the unlabeled set $\mathcal{X}_U$

$$\mathbf{X}^* = \arg\max_{\mathbf{X}\in\mathcal{X}_U} \alpha(\mathbf{X};\theta_A) \tag{2}$$

where an acquisition function $\alpha(\mathbf{X};\theta_A)$ is defined over input space to quantify the value of each unlabeled point. Here, one of the commonly used information-theoretic criteria is the entropy [50]. Specifically,

$$\begin{aligned}\alpha(\mathbf{X};\theta_A) &\triangleq \mathbb{H}[Y_{\mathbf{X}}|\mathbf{X};\theta_A] \\ &= -\sum_{i=1}^{N} p(Y_{\mathbf{X}}=i|\mathbf{X};\theta_A)\log p(Y_{\mathbf{X}}=i|\mathbf{X};\theta_A)\end{aligned} \tag{3}$$

where $Y_{\mathbf{X}}$ is the random variable representing the terrain class corresponding to the image patch X and $p(Y_{\mathbf{X}}=i|\mathbf{X};\theta_A)$ can be computed using the softmax layer of CNN classifier. At each iteration, the weight θ_A of the CNN classifier will be adapted. The unlabeled point of the highest entropy tends to have the highest predictive uncertainty. Thus, if such unlabeled points are annotated and used to train the GAN model, the generative samples can best reduce uncertainty of terrain classification.

C. Conditional Generative Adversarial Network

In order to handle multimodal data (e.g., multiple terrain classes), GAN can be extended to a CGAN [29] by letting both the generator G and discriminator D condition on some auxiliary information $\mathbf{c}$ (e.g., terrain classes). The objective function of CGAN can be defined as

$$\begin{aligned}&\min_{\theta_G}\max_{\theta_D} V_{CGAN}(G,D) \\ &\quad= \mathbb{E}_{\mathbf{X}\sim p_{\text{data}}}[\log D(\mathbf{X}|\mathbf{c})] + \mathbb{E}_{\mathbf{z}\sim p_{\text{noise}}} \\ &\qquad\times\big[\log(1-D(G(\mathbf{z}|\mathbf{c})))\big].\end{aligned} \tag{4}$$

In contrast to the CGAN model which has auxiliary information to both generator G and discriminator D, another conditional model called InfoGAN [28] can automatically learn the latent auxiliary representation. InfoGAN introduces an additional latent code $\mathbf{c}$ to the generator $G(\mathbf{z},\mathbf{c};\theta_G)$ where $\mathbf{z}$ is still the noise variable and $\mathbf{c}$ represents the semantic structure (e.g., terrain classes) in data. Unlike CGAN, this additional $\mathbf{c}$ follows a prior distribution $p(\mathbf{c})$. Then, a regularization term L is introduced to penalize low mutual information between distribution of latent code $\mathbf{c}$ and the generative distribution $\mathbf{X}\sim G(\mathbf{z},\mathbf{c};\theta_G)$. The regularization term L is defined as

$$L(G,Q) = \mathbb{E}_{\mathbf{c}\sim p(\mathbf{c}),\mathbf{X}\sim G(\mathbf{z},\mathbf{c})}\big[\log Q(\mathbf{c}|\mathbf{X})\big] \tag{5}$$

where $Q(\mathbf{c};\theta_Q)$ is a neural network approximating the posterior distribution $p(\mathbf{c}|\mathbf{X})$. The above term $L(G,Q)$ is an approximation of the lower bound of the mutual information $\mathbb{I}(\mathbf{c};\mathbf{X})$ (see [28] for the proof).

Then, the objective function of InfoGAN is defined by putting together the objective of original GAN V_{GAN} and an information-theoretic regularization term L parametrized by λ

$$\min_{\theta_G,\theta_Q}\max_{\theta_D} V_{InfoGAN}(D,G,Q) = V_{GAN}(D,G) - \lambda L(G,Q). \tag{6}$$

In the above three GAN models, the original GAN is an unconditional model which cannot handle multimodal data (e.g., the aerial images contain multiple terrain classes). In contrast, CGAN and InfoGAN can exploit auxiliary structure (i.e., terrain class or distribution of terrain class) to achieve better generative samples of multiple terrain classes. However, as shown in Fig. 1, the distributions of image patches from different terrain classes own different degrees of diversity in real world. Without a fine-grained modeling of the subclasses, we can expect poor generative samples by directly using CGAN and InfoGAN. To address this issue, we proposed two diversity-sensitive GAN models in Section III.

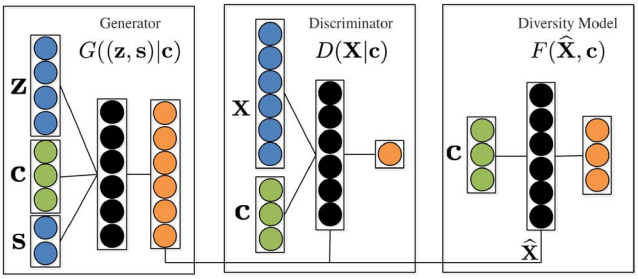

Fig. 4. Network structure of FcGAN.

III. Our Approaches

To model different degrees of diversity among terrain classes (see Fig. 1), this section introduces two novel CGAN models that can explicitly incorporate subclasses of terrain images.

A. Fine-Grained Conditional GAN

In the original CGAN model described in Section II-C, a simple auxiliary information $\mathbf{c}$ of terrain class is insufficient to capture the pattern of diversity among different terrains. Thus, we propose a fine-grained CGAN (FcGAN) model consisting of a generative model, a discriminative model, and an additional diversity model, which can automatically learn the distribution of subclasses given a certain terrain class. The network structure is shown in Fig. 4. The detail description of the components is as follows.

Generator: The generative model $G((\mathbf{z},\mathbf{s})|\mathbf{c};\theta_G)$ aims to generate samples that are indistinguishable from that sampled from the true condition data distribution $p_{\text{data}}(\mathbf{X}|\mathbf{c},\mathbf{s})$

where $\mathbf{z}$ is the noise variable, $\mathbf{c}$ models the terrain classes and $\mathbf{s}$ models the subclasses capturing the fine-grained underlying representation. In practice, the terrain classes $\mathbf{c}$ can be actively collected by system operators (see Fig. 2) and considered as known; the fine-grained representation $\mathbf{s}$ is learned automatically.

Discriminator: The discriminative model $D(\mathbf{X}|\mathbf{c};\theta_D)$ can also exploit terrain classes $\mathbf{c}$ to distinguish $\mathbf{X}$ as the true data or generated data with better accuracy.

Diversity Model: An additional model $Q(\mathbf{s}|\mathbf{X},\mathbf{c};\theta_Q)$ is designed to approximate posterior distribution $p(\mathbf{s}|\mathbf{X},\mathbf{c})$ of the fine-grained representation $\mathbf{s}$ given terrain images $\mathbf{X}$ of certain class $\mathbf{c}$. In order to learn the posterior distribution of fine-grained representation $\mathbf{s}$, an information-theoretic regularization is introduced as the mutual information $\mathbb{I}[\mathbf{s};G((\mathbf{z},\mathbf{s})|\mathbf{c})]$ between $\mathbf{s}$ and the generative distribution $G((\mathbf{z},\mathbf{s})|\mathbf{c})$. A high value of mutual information implies a high reduction of uncertainty in $\mathbf{s}$ given the generative samples obtained from $G((\mathbf{z},\mathbf{s})|\mathbf{c})$. However, the above term cannot be directly evaluated as we cannot access to the posterior distribution $p(\mathbf{s}|\mathbf{c},\mathbf{X})$. Thus, a lower bound can be derived using variational information maximization [51] to approximate the mutual information

$$\begin{aligned}
&\mathbb{I}[\mathbf{s};G((\mathbf{z},\mathbf{s})|\mathbf{c})]\\
&= \mathbb{H}[\mathbf{s}] - \mathbb{H}[\mathbf{s}|G((\mathbf{z},\mathbf{s})|\mathbf{c})]\\
&= \mathbb{E}_{\mathbf{X}\sim G((\mathbf{z},\mathbf{s})|\mathbf{c})}\big[\mathbb{E}_{\mathbf{s}'\sim p(\mathbf{s}|\mathbf{X},\mathbf{c})}\big[\log p\big(\mathbf{s}'|\mathbf{X},\mathbf{c}\big)\big]\big] + \mathbb{H}[\mathbf{s}]\\
&= \mathbb{E}_{\mathbf{X}\sim G((\mathbf{z},\mathbf{s})|\mathbf{c})}\left[\mathbb{E}_{\mathbf{s}'\sim p(\mathbf{s}|\mathbf{X},\mathbf{c})}\left[\log\frac{p(\mathbf{s}'|\mathbf{X},\mathbf{c})Q\big(\mathbf{s}'|\mathbf{X},\mathbf{c}\big)}{Q(\mathbf{s}'|\mathbf{X},\mathbf{c})}\right]\right] + \mathbb{H}[\mathbf{s}]\\
&= \mathbb{E}_{\mathbf{X}\sim G(\mathbf{z},\mathbf{s}|\mathbf{c})}\big[\mathbb{KL}\big[p\big(\mathbf{s}'|\mathbf{X},\mathbf{c}\big)\|Q\big(\mathbf{s}'|\mathbf{X},\mathbf{c}\big)\big]\big]\\
&\quad + \mathbb{E}_{\mathbf{X}\sim G((\mathbf{z},\mathbf{s})|\mathbf{c})}\big[\mathbb{E}_{\mathbf{s}'\sim p(\mathbf{s}|\mathbf{X},\mathbf{c})}\big[\log Q\big(\mathbf{s}'|\mathbf{X},\mathbf{c}\big)\big]\big] + \mathbb{H}[\mathbf{s}]\\
&\geq \mathbb{E}_{\mathbf{X}\sim G((\mathbf{z},\mathbf{s})|\mathbf{c})}\big[\mathbb{E}_{\mathbf{s}'\sim p(\mathbf{s}|\mathbf{X},\mathbf{c})}\big[\log Q\big(\mathbf{s}'|\mathbf{X},\mathbf{c}\big)\big]\big] + \mathbb{H}[\mathbf{s}]. \qquad (7)
\end{aligned}$$

In the above equation, given a prior distribution placed over $\mathbf{s}$, the entropy term $\mathbb{H}[\mathbf{s}]$ is a constant. However, it is difficult to compute the first term as the posterior distribution $p(\mathbf{s}|\mathbf{X},\mathbf{c})$ is not explicitly defined. To address this issue, an equivalent lower bound L_{FC} which is easier to compute can be derived as follows:

$$\begin{aligned}
L_{FC}(G,Q) &\triangleq \mathbb{E}_{\mathbf{s}\sim p(\mathbf{s}),\mathbf{X}\sim G((\mathbf{z},\mathbf{s})|\mathbf{c})}\big[\log Q(\mathbf{s}|\mathbf{X},\mathbf{c})\big] + \mathbb{H}(\mathbf{s})\\
&= \mathbb{E}_{\mathbf{s}\sim p(\mathbf{s}),\mathbf{X}\sim G((\mathbf{z},\mathbf{s})|\mathbf{c})}\big[\mathbb{E}_{\mathbf{s}'\sim p(\mathbf{s}|\mathbf{X},\mathbf{c})}\big[\log Q\big(\mathbf{s}'|\mathbf{X},\mathbf{c}\big)\big]\big]\\
&\quad + \mathbb{H}(\mathbf{s})\\
&= \mathbb{E}_{\mathbf{X}\sim G((\mathbf{z},\mathbf{s})|\mathbf{c})}\big[\mathbb{E}_{\mathbf{s}'\sim p(\mathbf{s}|\mathbf{X},\mathbf{c})}\big[\log Q\big(\mathbf{s}'|\mathbf{X},\mathbf{c}\big)\big]\big] + \mathbb{H}(\mathbf{s})\\
&\leq \mathbb{I}[\mathbf{s};G((\mathbf{z},\mathbf{s})|\mathbf{c})] \qquad (8)
\end{aligned}$$

Then, L_{FC} can now be evaluated using Monte Carlo simulation as $\mathbf{s}$ and $\mathbf{X}$ can be easily sampled. Putting together L_{FC} with the objective function of CGAN (4), we can define the objective function of the proposed FcGAN model which can be trained using min–max optimization

$$\begin{aligned}
&\min_{\theta_G,\theta_Q}\max_{\theta_D} V_{FcGAN}(G,D,Q)\\
&\quad\triangleq V_{CGAN}(G,D) - \lambda L_{FC}(G,Q)\\
&\quad\leq V_{CGAN}(G,D) - \lambda\mathbb{I}[\mathbf{s};G(\mathbf{z},\mathbf{s}|\mathbf{c})]. \qquad (9)
\end{aligned}$$

Algorithm 1 Active Terrain Mapping Coupled With FcGAN

Require: $\mathcal{M}$: CNN model
Require: $\mathcal{G}$: FcGAN model
Require: B: Number of annotated image patches in one iteration
Require: n: Total number of iterations
Require: $\mathcal{X}_L$: Set of human-labeled patches
Require: $\mathcal{X}_U$: Set of unlabeled patches

```
repeat
    Select top-B unlabeled patches from X_U ranked by AL strategy (2)
    Manually label the selected B-sized unlabeled patches and add into the set X_L
    Re-train G using (9) given the training set X_L
    Generate training samples using generator of the updated G models
    Re-train M using generative training samples
    Increase Iteration number by one
until Iteration number ≥ n
Build terrain map using M
```

The parameters θ_D, θ_G, and θ_Q in the objective function will be optimized so as to: 1) maximize the probability that the discriminator $D(\mathbf{X}|\mathbf{c};\theta_D)$ can distinguish the human-labeled terrain patches from the generative samples conditioning on certain terrain class $\mathbf{c}$; 2) minimize the probability that the generative samples from $G((\mathbf{z},\mathbf{s})|\mathbf{c};\theta_G)$ are identified by the discriminator $D(\mathbf{X}|\mathbf{c};\theta_D)$ as fake; and 3) maximize the uncertainty reduction in the distribution of fine-grained representation $\mathbf{s}$.

The proposed FcGAN can work with AL strategy to collect a more informative set of human-labeled terrain data. The detailed steps are shown in Algorithm 1.

B. Hierarchical InfoGAN for Automatic Terrain Generation

As we see in the previous section, FcGAN requires auxiliary information of terrain classes $\mathbf{c}$ to be manually collected which involves human intervention. This section introduces another novel GAN model that can remove the human intervention in FcGAN and address the diversity issue of terrain classes simultaneously. In contrast to the independence assumption of auxiliary variable $\mathbf{c}$ in the original InfoGAN model [28], we factorize the joint posterior distribution $p(\mathbf{c},\mathbf{s}|\widehat{\mathbf{X}})$ as the product of $p(\mathbf{c}|\widehat{\mathbf{X}})$ and $p(\mathbf{s}|\widehat{\mathbf{X}},\mathbf{c})$ which could better reflect the hierarchical patterns in terrain classes. We name this new hierarchical extension of InfoGAN as Hierarchical InfoGAN (HiGAN) and demonstrate its network structure in Fig. 5. We will describe each component in the following.

Generator: Unlike FcGAN treating coarse-grained terrain class $\mathbf{c}$ as known information, the generator of HiGAN $G(\mathbf{z},\mathbf{c},\mathbf{s};\theta_G)$ places prior distributions over both the coarse-grained structure $\mathbf{c}$ and the fine-grained structure $\mathbf{s}$. Then, the generator is inputted three random variables to generate samples reflecting the true data distribution p_{data}.

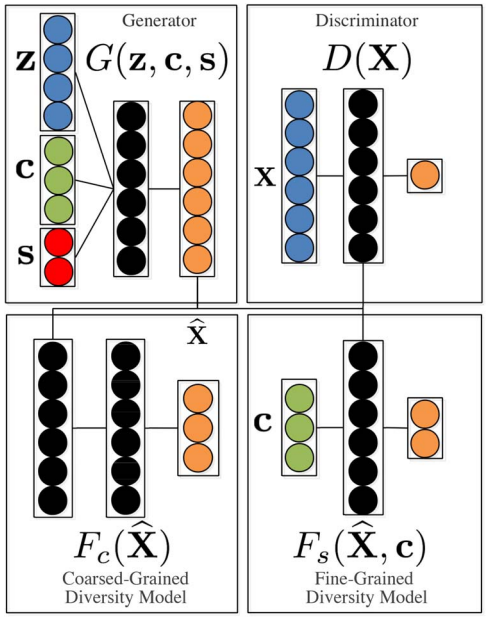

Fig. 5. Network structure of HiGAN.

Discriminator: Similar to the other GAN model, the discriminator $D(\mathbf{X}; \theta_D)$ aims to distinguish any input $\mathbf{X}$ as the true data or generative data.

Coarse-Grained Diversity Model: The posterior distribution of coarse-grained representation $p(\mathbf{c}|\widehat{\mathbf{X}})$ is approximated by a neural network $F_{cg}(\mathbf{c}|\widehat{\mathbf{X}}; \theta_{Q_{cg}})$ where $\theta_{Q_{cg}}$ are the network parameters and $\widehat{\mathbf{X}} \sim G$ represents generative samples.

Fine-grained Diversity Model: Similarly, the posterior distribution of fine-grained representation $p(\mathbf{s}|\widehat{\mathbf{X}}, \mathbf{c})$ is approximated by another neural network $F_{fg}(\mathbf{s}|\widehat{\mathbf{X}}, \mathbf{c}; \theta_{Q_{fg}})$ where $\theta_{Q_{fg}}$ are the network parameters and $\widehat{\mathbf{X}} \sim G$ represents generative samples.

In the next, we introduce the information-theoretic regularization which is defined as the mutual information between prior distribution $p(\mathbf{c}, \mathbf{s})$ and the generative model $G(\mathbf{z}, \mathbf{c}, \mathbf{s})$. As the mutual information cannot be computed analytically, to seek an approximated form, it can first be decomposed into simpler terms

$$\begin{aligned}
&\mathbb{I}[(\mathbf{c}, \mathbf{s}); G(\mathbf{z}, \mathbf{c}, \mathbf{s})] \\
&= \mathbb{H}[(\mathbf{c}, \mathbf{s})] - \mathbb{H}[(\mathbf{c}, \mathbf{s})|G(\mathbf{z}, \mathbf{c}, \mathbf{s})] \\
&= \mathbb{H}[(\mathbf{c}, \mathbf{s})] - \mathbb{H}[\mathbf{c}|G(\mathbf{z}, \mathbf{c}, \mathbf{s})] - \mathbb{H}[\mathbf{s}|\mathbf{c}, G(\mathbf{z}, \mathbf{c}, \mathbf{s})] \qquad (10)
\end{aligned}$$

where the first equality uses the property of mutual information $\mathbb{I}[(X, Y); Z] = \mathbb{H}[X, Y] - \mathbb{H}[X, Y|Z]$ and the second equation is due to the property of conditional entropy $\mathbb{H}[X, Y|Z] = \mathbb{H}[X|Z] + \mathbb{H}[Y|X, Z]$. Then, the mutual information can be decomposed into three entropy terms.

Given a proper prior distribution $p(\mathbf{c}, \mathbf{s})$, the first term is a constant. The second term and third term are difficult to compute as we have no access to $p(\mathbf{c}|\widehat{\mathbf{X}})$ and $p(\mathbf{s}|\mathbf{c}, \widehat{\mathbf{X}})$. To address this issue, we can first derive the lower bounds for the second and third terms, respectively,

$$\begin{aligned}
&-\mathbb{H}[\mathbf{c}|G(\mathbf{z}, \mathbf{c}, \mathbf{s})] \\
&= \mathbb{E}_{\mathbf{X}\sim G(\mathbf{z},\mathbf{c},\mathbf{s})}\big[\mathbb{E}_{\mathbf{c}'\sim p(\mathbf{c}|\mathbf{X})}\big[\log p\big(\mathbf{c}'|\mathbf{X}\big)\big]\big] \\
&= \mathbb{E}_{\mathbf{X}\sim G(\mathbf{z},\mathbf{c},\mathbf{s})}\left[\mathbb{E}_{\mathbf{c}'\sim p(\mathbf{c}|\mathbf{X})}\left[\log \frac{p\big(\mathbf{c}'|\mathbf{X}\big)Q_c\big(\mathbf{c}'|\mathbf{X}\big)}{Q_c\big(\mathbf{c}'|\mathbf{X}\big)}\right]\right] \\
&= \mathbb{E}_{\mathbf{X}\sim G(\mathbf{z},\mathbf{c},\mathbf{s}))}\big[\mathbb{KL}\big[p\big(\mathbf{c}'|\mathbf{X}\big); Q_c\big(\mathbf{c}'|\mathbf{X}\big)\big]\big] \\
&\quad + \mathbb{E}_{\mathbf{X}\sim G(\mathbf{z},\mathbf{c},\mathbf{s})}\big[\mathbb{E}_{\mathbf{c}'\sim p(\mathbf{c}|\mathbf{X})}\big[\log Q_c\big(\mathbf{c}'|\mathbf{X}\big)\big]\big] \\
&\geq \mathbb{E}_{\mathbf{X}\sim G(\mathbf{z},\mathbf{c},\mathbf{s})}\big[\mathbb{E}_{\mathbf{c}'\sim p(\mathbf{c}|\mathbf{X})}\big[\log Q_c\big(\mathbf{c}'|\mathbf{X}\big)\big]\big]. \qquad (11)
\end{aligned}$$

$$\begin{aligned}
&-\mathbb{H}[\mathbf{s}|\mathbf{c}, G(\mathbf{z}, \mathbf{c}, \mathbf{s})] \\
&= \mathbb{E}_{\mathbf{X}\sim G(\mathbf{z},\mathbf{c},\mathbf{s}))}\big[\mathbb{E}_{\mathbf{c}'\sim p(\mathbf{c}|\mathbf{X}),\mathbf{s}'\sim p(\mathbf{s}|\mathbf{c}',\mathbf{X})}\big[\log p\big(\mathbf{s}'|\mathbf{c}', \mathbf{X}\big)\big]\big] \\
&= \mathbb{E}_{\mathbf{X}\sim G(\mathbf{z},\mathbf{c},\mathbf{s}))}\Bigg[\mathbb{E}_{\mathbf{c}'\sim p(\mathbf{c}|\mathbf{X}),\mathbf{s}'\sim p(\mathbf{s}|\mathbf{c}',\mathbf{X})} \\
&\qquad \times \left[\log \frac{p\big(\mathbf{s}'|\mathbf{X}, \mathbf{c}'\big)Q_s\big(\mathbf{s}'|\mathbf{X}, \mathbf{c}'\big)}{Q_s\big(\mathbf{s}'|\mathbf{X}, \mathbf{c}'\big)}\right]\Bigg] \\
&= \mathbb{E}_{\mathbf{X}\sim G(\mathbf{z},\mathbf{c},\mathbf{s}))}\big[\mathbb{E}_{\mathbf{c}'\sim p(\mathbf{c}|\mathbf{X})}\big[\mathbb{KL}\big[p\big(\mathbf{s}'|\mathbf{X}, \mathbf{c}'\big); Q_s\big(\mathbf{s}'|\mathbf{X}, \mathbf{c}'\big)\big]\big]\big] \\
&\quad + \mathbb{E}_{\mathbf{X}\sim G(\mathbf{z},\mathbf{c},\mathbf{s})}\big[\mathbb{E}_{\mathbf{c}'\sim p(\mathbf{c}|\mathbf{X}),\mathbf{s}'\sim p(\mathbf{s}|\mathbf{c}',\mathbf{X})}\big[\log Q_s\big(\mathbf{s}'|\mathbf{X}, \mathbf{c}'\big)\big]\big] \\
&\geq \mathbb{E}_{\mathbf{X}\sim G(\mathbf{z},\mathbf{c},\mathbf{s}))}\big[\mathbb{E}_{\mathbf{c}'\sim p(\mathbf{c}|\mathbf{X}),\mathbf{s}'\sim p(\mathbf{s}|\mathbf{c}',\mathbf{X})}\big[\log Q_s\big(\mathbf{s}'|\mathbf{X}, \mathbf{c}'\big)\big]\big]. \qquad (12)
\end{aligned}$$

In the above equations, two auxiliary distributions $Q_c(\mathbf{c}|\widehat{\mathbf{X}})$ and $Q_s(\mathbf{s}|\mathbf{c}, \widehat{\mathbf{X}})$ are used to approximate two posterior distributions, respectively. However, the lower bound cannot be computed as it still requires to sample the posterior distribution $p(\mathbf{c}|\mathbf{X})$ and $p(\mathbf{s}|\mathbf{c}, \mathbf{X})$. To address this issue, we derive the equivalence of the lower bound which can be evaluated. The equivalent expressions of the above two lower bounds are denoted as L_C and L_S as follows:

$$\begin{aligned}
&L_C(G(\mathbf{z}, \mathbf{c}, \mathbf{s}), Q_c) \\
&\quad \triangleq \mathbb{E}_{\mathbf{c}\sim p(\mathbf{c}),\mathbf{X}\sim G(\mathbf{z},\mathbf{c},\mathbf{s})}\big[\log Q_c(\mathbf{c}|\mathbf{X})\big] \\
&\quad = \mathbb{E}_{\mathbf{X}\sim G(\mathbf{z},\mathbf{c},\mathbf{s})}\big[\mathbb{E}_{\mathbf{c}'\sim p(\mathbf{c}|\mathbf{X})}\big[\log Q_c\big(\mathbf{c}'|\mathbf{X}\big)\big]\big] \\
&\leq -\mathbb{H}[\mathbf{c}|G(\mathbf{z}, \mathbf{c}, \mathbf{s})]. \qquad (13) \\
&\quad L_S[G(\mathbf{z}, \mathbf{c}, \mathbf{s}), Q_s] \\
&\quad \triangleq \mathbb{E}_{\mathbf{c}\sim p(\mathbf{c}),\mathbf{s}\sim p(\mathbf{s}|\mathbf{c}),\mathbf{X}\sim G(\mathbf{z},\mathbf{c},\mathbf{s})}\big[\log Q_s(\mathbf{s}|\mathbf{X}, \mathbf{c})\big] \\
&\quad = \mathbb{E}_{\mathbf{X}\sim G(\mathbf{z},\mathbf{c},\mathbf{s})}\big[\mathbb{E}_{\mathbf{c}'\sim p(\mathbf{c}|\mathbf{X}),\mathbf{s}'\sim p(\mathbf{s}|\mathbf{c}',\mathbf{X})}\big[\log Q_s\big(\mathbf{s}'|\mathbf{X}, \mathbf{c}'\big)\big]\big] \\
&\quad \leq -\mathbb{H}[\mathbf{s}|\mathbf{c}, G(\mathbf{z}, \mathbf{c}, \mathbf{s})]. \qquad (14)
\end{aligned}$$

As $p(\mathbf{c})$ and $p(\mathbf{s}|\mathbf{c})$ can be some known prior distributions, $L(G, Q_{cg})$ and $L(G, Q_s)$ can be evaluated using Monte Carlo simulation. Putting together the objective function of the GAN model, the above two terms and entropy term $\mathbb{H}[\mathbf{c}, \mathbf{s}]$, the proposed HiGAN aims to optimize the model parameters θ_G, θ_D, θ_{Q_c}, and θ_{Q_s} by playing the following minmax game:

$$\begin{aligned}
&\min_{\theta_G,\theta_{Q_c},\theta_{Q_s}} \max_{\theta_D} V_{HiGAN}(G, D, Q_c, Q_s) \\
&\quad \triangleq V_{GAN}(G, D) - \lambda(L_C(G, Q_c) - L_S(G, Q_s) + \mathbb{H}[\mathbf{c}, \mathbf{s}]) \\
&\quad \leq V_{GAN}(G, D) - \lambda\mathbb{I}[(\mathbf{c}, \mathbf{s})|G(\mathbf{z}, \mathbf{c}, \mathbf{s})]. \qquad (15)
\end{aligned}$$

In the above equation, the second inequality is due to (10)–(14). In this new formulation, the generator G aims to generate samples that have minimum probability of being identified by the discriminator D and maximum reduction of uncertainty in joint diversity model $p(\mathbf{c}, \mathbf{s})$. The proposed HiGAN can also be coupled with AL strategy to perform automatic terrain mapping (see Algorithm 2).

Algorithm 2 Automatic Terrain Mapping Based on HiGAN

Require: $\mathcal{M}$: CNN model
Require: $\mathcal{G}$: HiGAN model
Require: B: Number of selected image patches in one iteration
Require: n: Total number of iterations
Require: $\mathcal{X}_U$: Set of unlabeled patches
1: **repeat**
2: Select top-B unlabeled patches from $\mathcal{X}_U$ ranked by AL strategy (2)
3: Re-train $\mathcal{G}$ using (15) given the selected B-sized batch of unlabeled patches
4: Obtain the generative training samples using the generator of updated $\mathcal{G}$ models
5: Determine the terrain classes corresponding to each element of **c**
6: Re-train $\mathcal{M}$ using generative training samples from each terrain class
7: Increase Iteration number by one
8: **until** Iteration number $\geq n$
9: Build terrain map using $\mathcal{M}$

(a) (b)

Fig. 6. Hardware of the collaborative air–ground robotic platform. (a) UAV. (b) UGV.

IV. Experiments and Results

A. Implementation of the Collaborative Air–Ground Robotic System

Hardware System: The proposed algorithms are tested in our collaborative air–ground robotic platform which consists of UAV, UGV, and ground station (GS). The UAV is a DJI Inspire 1 Pro equipped with camera DJI Zenmuse X5 [see Fig. 6(a)]. The UGV is a four-wheeled Autolabor Pro with an on-board computer Nvidia TX2 mounted with multiple sensors (e.g., a gyroscope, accelerometer, electronic compass, and rplidar A1) for localization [see Fig. 6(b)]. The GS is a computer mounted with Intel i5 CPU, 16GB RAM, and NVIDIA Tesla P100 GPU.

Software System: The proposed framework will run distributedly among the computing nodes mounted on UAV, UGV, and GS [52]–[55]. The software architecture is shown in Fig. 7. The UAV subsystem is designed to collect the aerial images using the on-board camera and transmit the data to the GS. Then, the GS subsystem runs the terrain mapping algorithm which conducts computational intensive tasks, such as aerial image preprocessing, active annotation, sample generation, and training model (i.e., CNN and GAN); it is also responsible for the data visualization and interaction with users (e.g., overriding the control in unexpected situations). Finally, the UGV subsystem receives the terrain map from the GS and integrates the terrain map with the local map for ground path planning. All nodes in the system run the tasks and communicate in the robot operating system (ROS)[2] environment.

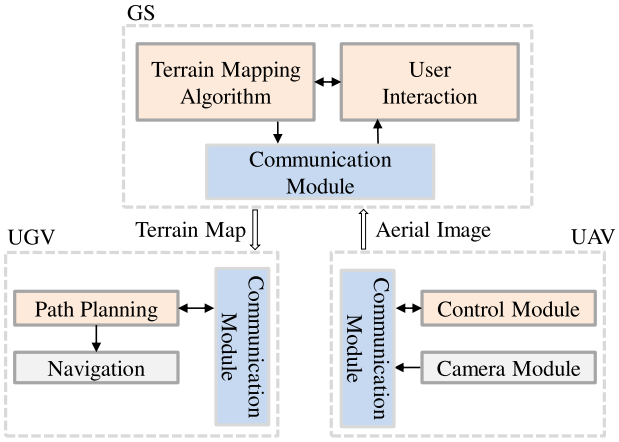

Fig. 7. Software of the collaborative air–ground robotic system.

(a) (b)

Fig. 8. Aerial view of testing ground in South Campus of Shenzhen University. (a) Roof area. (b) Pedestrian area.

B. Experimental Setting

Data Collection: To test the proposed algorithms, the UAV is tasked to collect aerial images (4200×2560 in pixel) in a roof area and a pedestrian area in the South Campus of Shenzhen University (see Fig. 8).

Comparison: The proposed FcGAN (Section III-A) and HiGAN (Section III-B) will be compared with their existing counterparts: 1) Non-GAN model [5] which exploits the traditional data augmentation method to generate samples; 2) original GAN model [20]; 3) CGAN model [29]; and 4) InfoGAN model [28]. In addition, the proposed terrain mapping framework (Section II-C) can work with *Random* or *Active* selection of patches for training the above GAN models.

Performance Metric: The performance of algorithms can be evaluated in terms of predictive accuracy, visual quality of terrain mapping, and average length of the planned path for UGV.

C. Accuracy of Terrain Classification

In the first experiment, we aim to evaluate the performance of the proposed FcGAN. Here, the unlabeled patches are

[2]http://www.ros.org

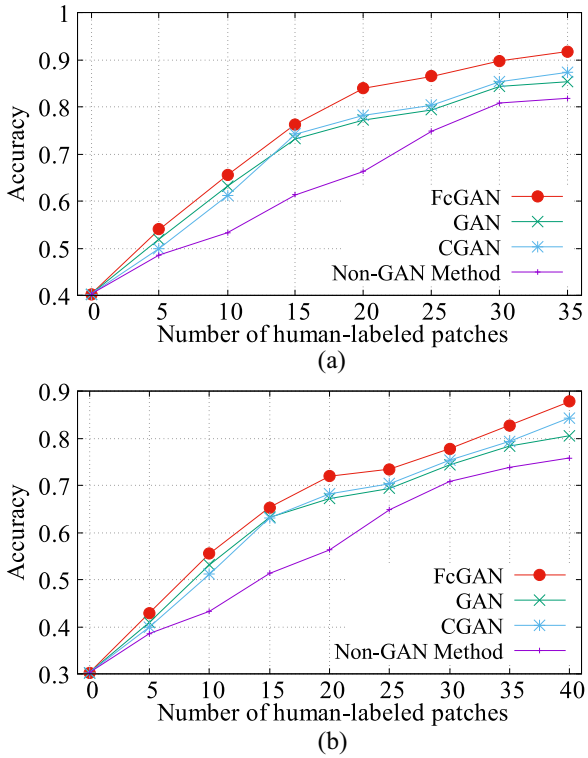

Fig. 9. Predictive accuracy of terrain classification based on random patch selection. (a) Roof area. (b) Pedestrian area.

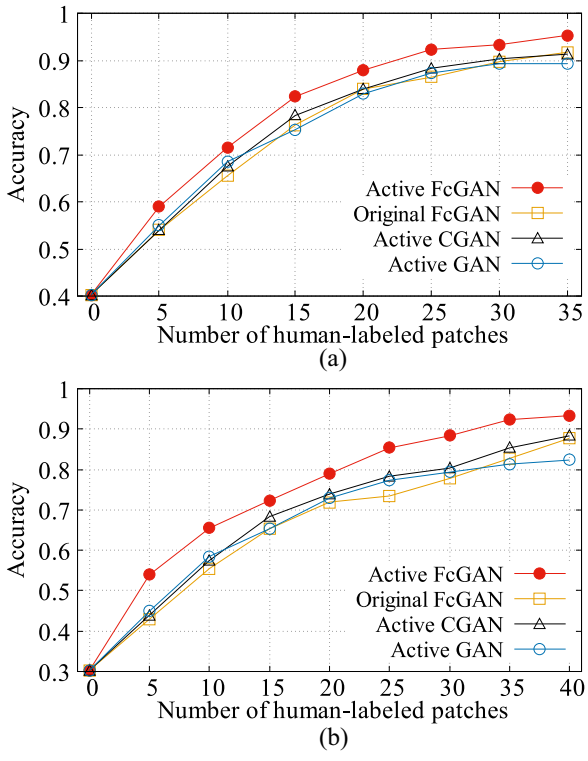

Fig. 10. Predictive accuracy of active terrain classification based on GAN models. (a) Roof area. (b) Pedestrian area.

randomly selected and labeled to train the generative models, which then generate image patches to train the CNN terrain classifier. As shown in Fig. 9, FcGAN outperforms the other three approaches including its GAN-based counterparts.

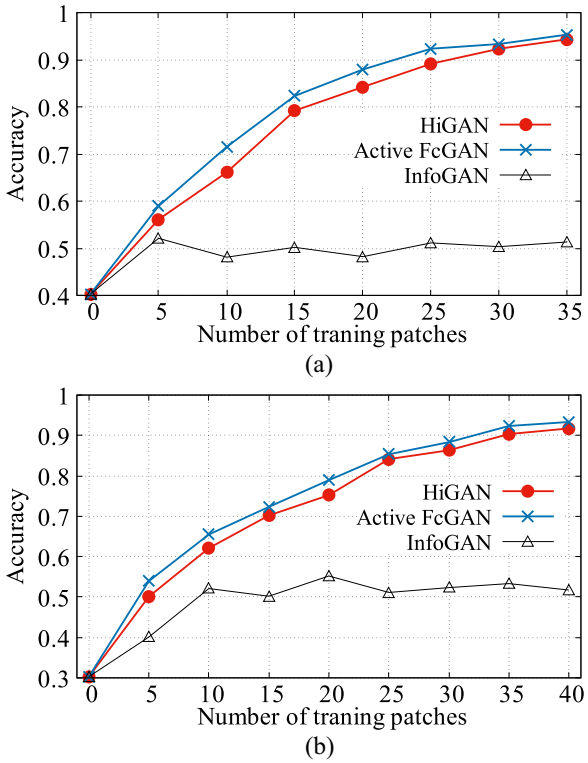

Fig. 11. Predictive accuracy of automatic terrain classification. (a) Roof area. (b) Pedestrian area.

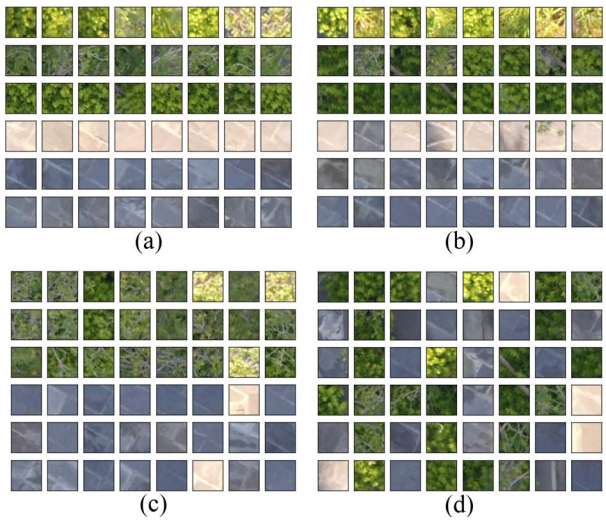

Fig. 12. Terrain patches generated from various GAN models. (a) FcGAN. (b) HiGAN. (c) CGAN. (d) InfoGAN.

This indicates that the fine-grained diversity model allows FcGAN to generate better image patches for training terrain classifier.

The AL strategy is then included in the second experiment to actively select the unlabeled patches for labeling. The rest parts of the experiments are kept the same. Fig. 10 shows that the AL strategy can further improve the performance of FcGAN. In addition, the CGAN and GAN models coupled with active selection now can achieve comparable predictive accuracy as the original FcGAN. The results imply that the

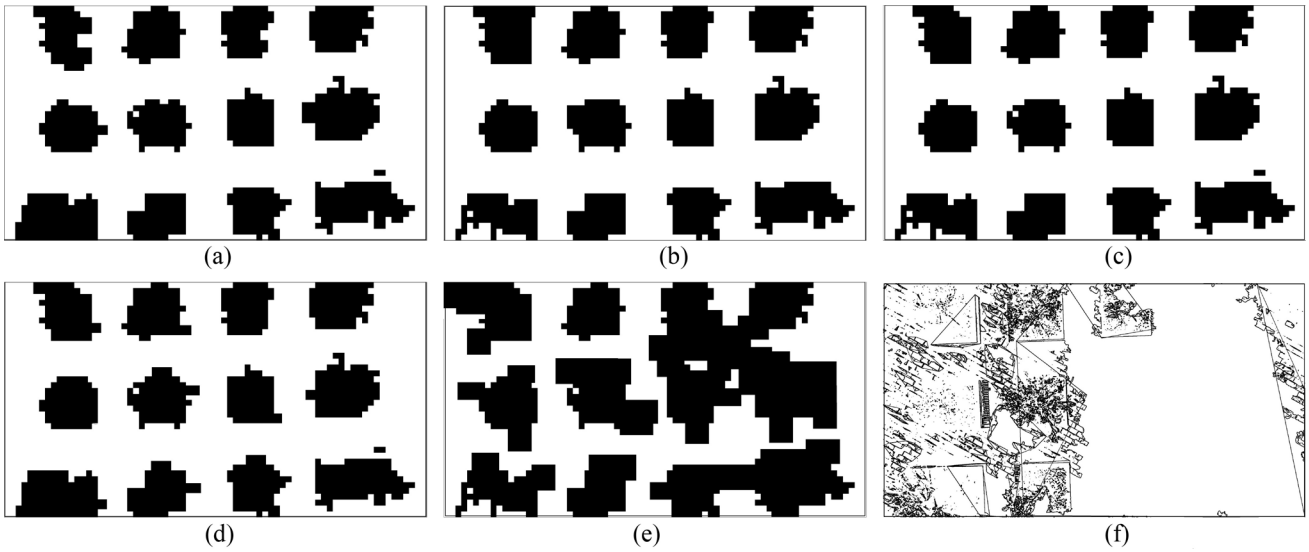

Fig. 13. Terrain mapping using various approaches in roof area. (a) FcGAN. (b) Active FcGAN. (c) HiGAN. (d) CGAN. (e) InfoGAN. (f) Edge detection.

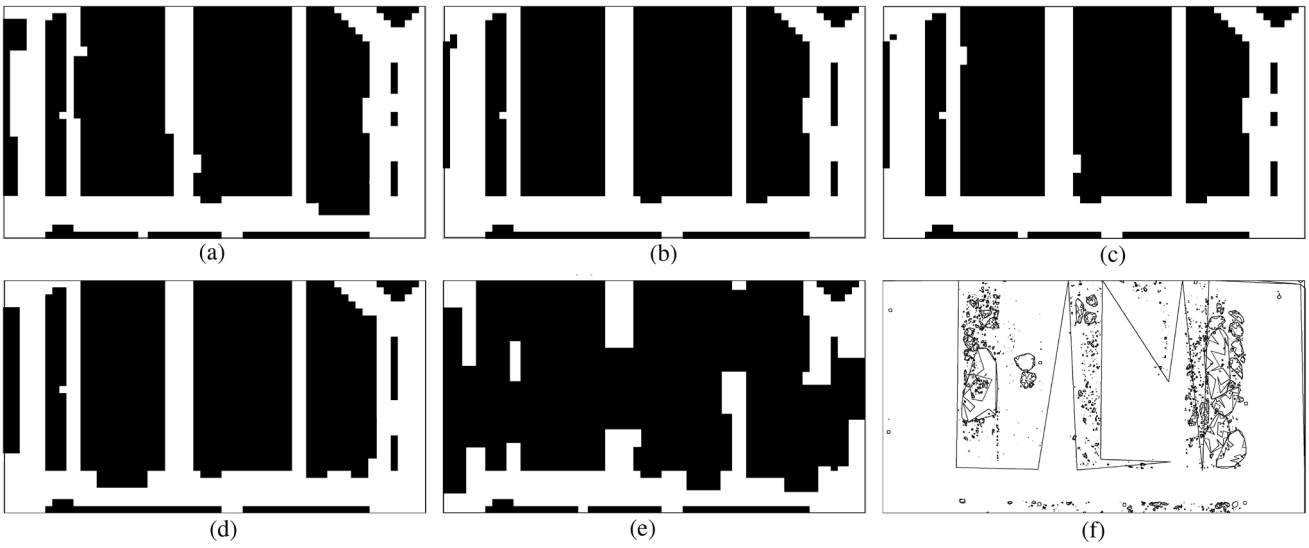

Fig. 14. Terrain mapping using various approaches in pedestrian area. (a) FcGAN. (b) Active FcGAN. (c) HiGAN. (d) CGAN. (e) InfoGAN. (f) Edge detection.

AL strategy can be especially useful when human intervention (e.g., labeling) is limited as it allows to use less data (more informative) for training GAN models.

The third experiment aims to test the automatic terrain classification based on HiGAN which does not rely on human-labeled patches. Fig. 11 shows that HiGAN outperforms InfoGAN significantly. This indicates that the coarse-grained and fine-grained diversity models can effectively capture the diversity pattern in terrain classes. We can also observe that HiGAN is slightly worse than Active FcGAN because it uses much less human intervention. Thus, HiGAN could be a valuable choice when human resource is extremely scarce or expensive.

The final experiment demonstrates the generative samples obtained from various GAN models (Fig. 12). It can be clearly observed that HiGAN and FcGAN can generate image patches that reflect the diverse terrain patterns in Fig. 8(b). The observation also explains the better performance of HiGAN and FcGAN when compared with their counterparts.

D. Quality of Terrain Mapping

As the terrain map based on the aerial image will be integrated with the local map of the ground robot, it is necessary to investigate the quality visually. As demonstrated in Figs. 13 and 14, the proposed approaches can achieve clear terrain maps that match the real aerial images in both scenarios (Fig. 8). The traditional edge detection and polygonal approximation [10] works poorly in both scenarios due to complex environmental conditions (e.g., light intensity). The InfoGAN model also works poorly as it cannot well model the diversity pattern in the terrain classes.

In addition, we evaluate the performance of the proposed approaches on video stream data as shown in Fig. 15. The number of patches for training GAN models varies as 10, 20,

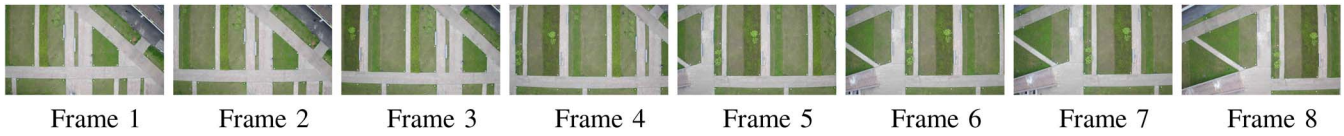

Fig. 15. Aerial images extracted from video stream in the pedestrian area.

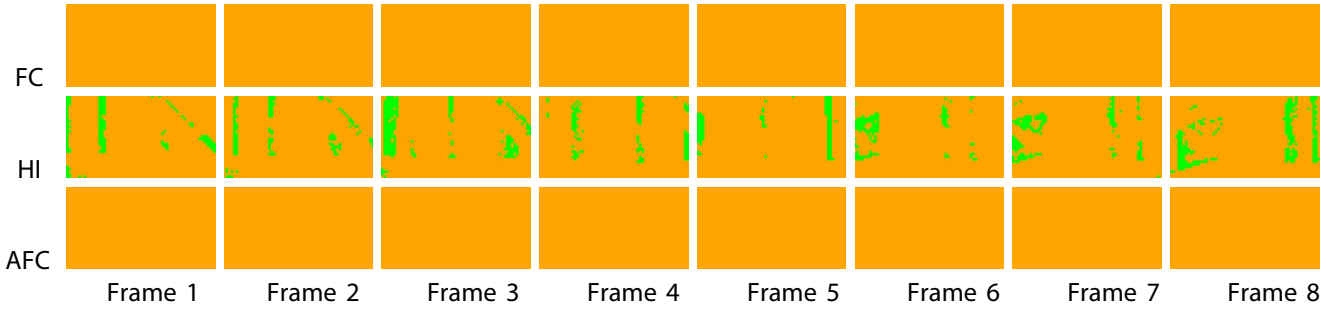

Fig. 16. Comparison of HiGAN (HI), FcGAN (FC), and Active FcGAN (AFC) in terrain mapping with 10 terrain patches.

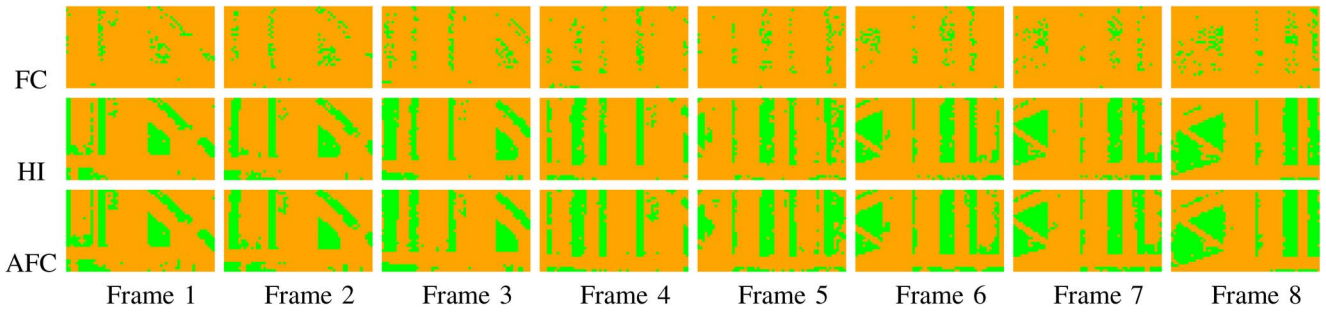

Fig. 17. Comparison of HiGAN (HI), FcGAN (FC), and Active FcGAN (AFC) in terrain mapping with 20 terrain patches.

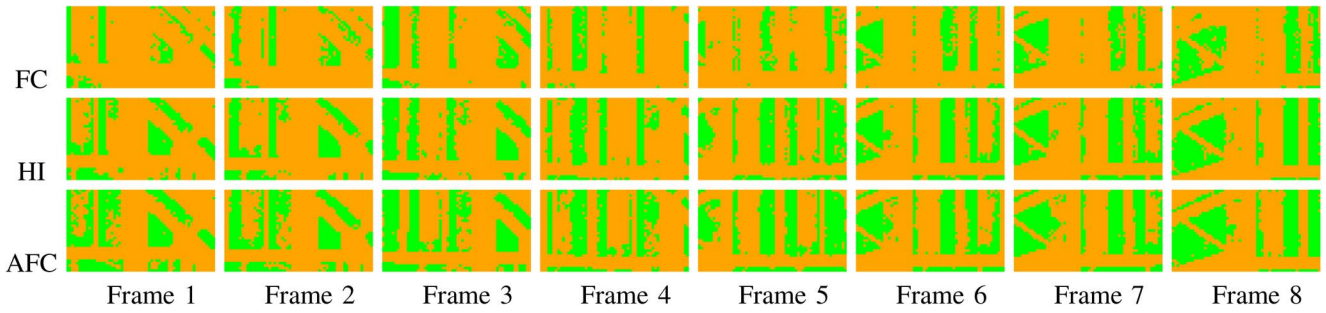

Fig. 18. Comparison of HiGAN (HI), FcGAN (FC), and Active FcGAN (AFC) in terrain mapping with 30 terrain patches.

30, and 40. As we can see in Fig. 16, HiGAN performs better than the other two models because FcGAN relies on some human-labeled training data. From Fig. 17 to Fig. 18, we can observe that both HiGAN and Active FcGAN are significantly better than nonActive FcGAN; Active FcGAN is sightly better than HiGAN (e.g., see frame 1 and frame 2). All three models can obtain a visually comparable good terrain map when the number of patches is 40 (see Fig. 19). The above results imply that HiGAN is a better choice when human-labeled patches are extremely limited and Active FcGAN can achieve the best overall performance in practice.

E. Evaluation of Ground Path Planning

The final experiments evaluate the performance of ground path planning using the terrain mapping built by various models. The original and destination points of the UGV is randomly picked in the terrain map. Then, ground path planning is performed using the rapid exploring random tree (RRT) algorithm [56] which has been widely used in autonomous motion planning. The average length of the planned path will be used to evaluate the performance of the terrain mapping algorithm.

As we can see in Table II, the Active FcGAN can plan the shortest path with an average length which is 1389.7 and 1481.2 pt in the roof and pedestrian data, respectively. Though HiGAN is slightly worse than the Active FcGAN, it still achieves comparable results: the shortest paths are with the average length as 1395.1 and 1500.3 pt in roof and pedestrian data, respectively. The results are expected based on the analysis from the previous experiments.

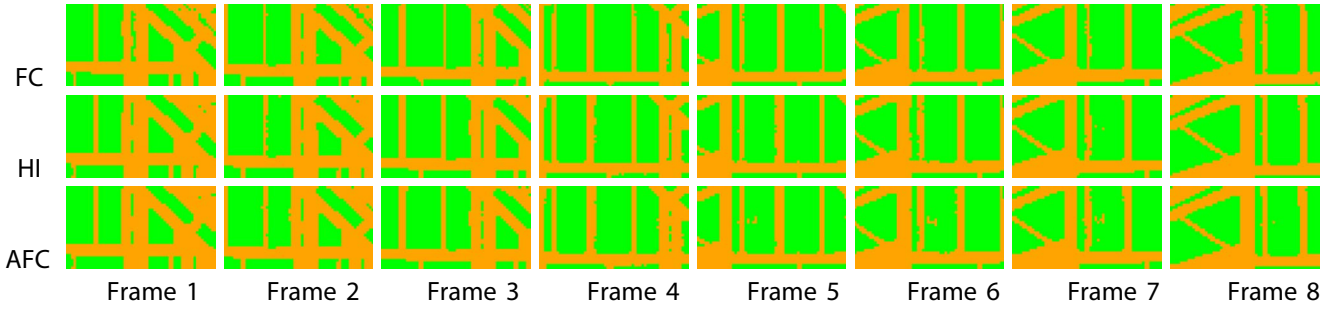

Fig. 19. Comparison of HiGAN (HI), FcGAN (FC), and Active FcGAN (AFC) in terrain mapping with 40 terrain patches.

TABLE II
AVERAGE LENGTH OF GROUND PATH PLANNING BASED ON TERRAIN MAPPING USING VARIOUS GENERATIVE METHODS

Model / Avg. Length (pt)	Non-GAN	GAN	CGAN	FcGAN	InfoGAN	Active GAN	Active CGAN	Active FcGAN	HiGAN
Roof Area	1901.4	1866.7	1621.4	1468.1	1989.7	1475.4	1465.4	**1389.7**	1395.1
Pedestrian Area	2401.4	2165.1	2090.1	1566.9	2681.3	1575.1	1531.2	**1481.2**	1500.3

V. CONCLUSION

The collaborative air–ground robotic system has shown potential in many urban applications. As one of the key functionalities, terrain mapping using aerial images can offer a large-scale view of the field for the ground robot to plan a globally optimal path. This article proposes the terrain mapping framework which integrates both AL strategy and GAN models to collect/use a limited human-labeled data effectively. Furthermore, two diversity-sensitive GAN models (i.e., FcGAN and HiGAN) are proposed to improve the generation quality of terrain data based on fine-grained modeling of diversity patterns among terrain data. Our approach is especially useful during real-world deployment in a novel environment where human intervention is costly and limited. To make the system more realistic, we will investigate online map fusion among aerial images and multiple sensors on ground in our future work.

REFERENCES

[1] N. Mohamed, J. Al-Jaroodi, I. Jawhar, A. Idries, and F. Mohammed, "Unmanned aerial vehicles applications in future smart cities," *Technol. Forecast. Soc. Change*, Sep. 2018, Art. no. 119293. [Online]. Available: https://www.sciencedirect.com/science/article/pii/S0040162517314968

[2] J.-Q. Li, F. R. Yu, G. Deng, C. Luo, Z. Ming, and Q. Yan, "Industrial Internet: A survey on the enabling technologies, applications, and challenges," *IEEE Commun. Surveys Tuts.*, vol. 19, no. 3, pp. 1504–1526, 3rd Quart., 2017.

[3] H. S. M. Lim and A. Taeihagh, "Autonomous vehicles for smart and sustainable cities: An in-depth exploration of privacy and cybersecurity implications," *Energies*, vol. 11, no. 5, p. 1062, 2018.

[4] X. Liu, W. Liu, H. Ma, and H. Fu, "Large-scale vehicle re-identification in urban surveillance videos," in *Proc. IEEE Int. Conf. Multimedia Expo (ICME)*, 2016, pp. 1–6.

[5] J. Delmerico, A. Giusti, E. Mueggler, L. M. Gambardella, and D. Scaramuzza, "'On-the-spot training' for terrain classification in autonomous air-ground collaborative teams," in *Proc. Int. Symp. Exp. Robot.*, 2016, pp. 574–585.

[6] J. Peterson, H. Chaudhry, K. Abdelatty, J. Bird, and K. Kochersberger, "Online aerial terrain mapping for ground robot navigation," *Sensors*, vol. 18, no. 2, p. 630, 2018.

[7] G. Christie, A. Shoemaker, K. Kochersberger, P. Tokekar, L. Mclean, and A. Leonessa, "Radiation search operations using scene understanding with autonomous UAV and UGV," *J. Field Robot.*, vol. 34, no. 8, pp. 1450–1468, 2017.

[8] J. Delmerico, E. Mueggler, J. Nitsch, and D. Scaramuzza, "Active autonomous aerial exploration for ground robot path planning," *IEEE Robot. Autom. Lett.*, vol. 2, no. 2, pp. 664–671, Apr. 2017.

[9] B. Sofman, E. Lin, J. A. Bagnell, J. Cole, N. Vandapel, and A. Stentz, "Improving robot navigation through self-supervised online learning," *J. Field Robot.*, vol. 23, nos. 11–12, pp. 1059–1075, 2006.

[10] J. Li, G. Deng, C. Luo, Q. Lin, Y. Qiao, and M. Zhong, "A hybrid path planning method in unmanned air/ground vehicle (UAV/UGV) cooperative systems," *IEEE Trans. Veh. Technol.*, vol. 65, no. 12, pp. 9585–9596, Dec. 2016.

[11] K. Fregene, D. Kennedy, R. Madhavan, L. E. Parker, and D. Wang, "A class of intelligent agents for coordinated control of outdoor terrain mapping UGVs," *Eng. Appl. Artif. Intell.*, vol. 18, no. 5, pp. 513–531, 2005.

[12] K. Otsu, M. Ono, T. J. Fuchs, I. Baldwin, and T. Kubota, "Autonomous terrain classification with co-and self-training approach," *IEEE Robot. Autom. Lett.*, vol. 1, no. 2, pp. 814–819, Jul. 2016.

[13] K. Walas, "Terrain classification and negotiation with a walking robot," *J. Intell. Robot. Syst.*, vol. 78, nos. 3–4, pp. 401–423, 2015.

[14] K. Otsu and T. Kubota, "Energy-aware terrain analysis for mobile robot exploration," in *Proc. FSR*, 2016, pp. 373–388.

[15] C. Ye, "Navigating a mobile robot by a traversability field histogram," *IEEE Trans. Syst., Man, Cybern. B, Cybern.*, vol. 37, no. 2, pp. 361–372, Apr. 2007.

[16] M. Ono, T. J. Fuchs, A. Steffy, M. Maimone, and J. Yen, "Risk-aware planetary rover operation: Autonomous terrain classification and path planning," in *Proc. IEEE Aerosp. Conf.*, 2015, pp. 1–10.

[17] C. Castejón, D. Blanco, and L. Moreno, "Compact modeling technique for outdoor navigation," *IEEE Trans. Syst., Man, Cybern. B, Cybern.*, vol. 38, no. 1, pp. 9–24, Jan. 2008.

[18] J. Long, E. Shelhamer, and T. Darrell, "Fully convolutional networks for semantic segmentation," in *Proc. IEEE Conf. Comput. Vis. Pattern Recognit.*, 2015, pp. 3431–3440.

[19] B. Sofman, J. Bagnell, A. Stentz, and N. Vandapel, "Terrain classification from aerial data to support ground vehicle navigation," Robot. Inst., Carnegie Mellon Univ., Rep. CMURI-TR-05-39, 2006.

[20] I. J. Goodfellow *et al.*, "Generative adversarial nets," in *Proc. Adv. Neural Inf. Process. Syst.*, 2014, pp. 2672–2680.

[21] J. Deng, W. Dong, R. Socher, L.-J. Li, K. Li, and L. Fei-Fei, "ImageNet: A large-scale hierarchical image database," in *Proc. IEEE Conf. Comput. Vis. Pattern Recognit.*, 2009, pp. 248–255.

[22] Z. Zhong, J. Li, D. A. Clausi, and A. Wong, "Generative adversarial networks and conditional random fields for hyperspectral image classification," *IEEE Trans. Cybern.*, to be published.

[23] S. Gurumurthy, R. K. Sarvadevabhatla, and R. V. Babu, "DeLiGAN: Generative adversarial networks for diverse and limited data," in *Proc. IEEE Conf. Comput. Vis. Pattern Recognit.*, 2017, pp. 166–174.

[24] H. Shi, L. Wang, G. Ding, F. Yang, and X. Li, "Data augmentation with improved generative adversarial networks," in *Proc. ICPR*, 2018, pp. 73–78.

[25] J. Zhang, Y. Peng, and M. Yuan, "SCH-GAN: Semi-supervised cross-modal hashing by generative adversarial network," *IEEE Trans. Cybern.*, vol. 50, no. 2, pp. 489–502, Feb. 2020. [Online]. Available: https://ieeexplore.ieee.org/document/8472802

[26] A. Antoniou, A. Storkey, and H. Edwards, "Augmenting image classifiers using data augmentation generative adversarial networks," in *Proc. ICANN*, 2018, pp. 594–603.

[27] A. Radford, L. Metz, and S. Chintala, "Unsupervised representation learning with deep convolutional generative adversarial networks," in *Proc. ICLR*, 2015, pp. 248–255.

[28] X. Chen, Y. Duan, R. Houthooft, J. Schulman, I. Sutskever, and P. Abbeel, "InfoGAN: Interpretable representation learning by information maximizing generative adversarial nets," in *Proc. Adv. Neural Inf. Process. Syst.*, 2016, pp. 2172–2180.

[29] M. Mirza and S. Osindero, "Conditional generative adversarial nets," 2014. [Online]. Available: arXiv:1411.1784

[30] A. J. Joshi, F. Porikli, and N. Papanikolopoulos, "Multi-class active learning for image classification," in *Proc. IEEE Conf. Comput. Vis. Pattern Recognit.*, 2009, pp. 2372–2379.

[31] L. Xin and Y. Guo, "Adaptive active learning for image classification," in *Proc. IEEE Conf. Comput. Vis. Pattern Recognit.*, 2013, pp. 859–866.

[32] B. Du *et al.*, "Exploring representativeness and informativeness for active learning," *IEEE Trans. Cybern.*, vol. 47, no. 1, pp. 14–26, Jan. 2017.

[33] Z. Qiu, D. J. Miller, and G. Kesidis, "A maximum entropy framework for semisupervised and active learning with unknown and label-scarce classes," *IEEE Trans. Neural Netw. Learn. Syst.*, vol. 28, no. 4, pp. 917–933, Apr. 2017.

[34] K. H. Low, J. Chen, J. M. Dolan, S. A. Chien, and D. R. Thompson, "Decentralized active robotic exploration and mapping for probabilistic field classification in environmental sensing," in *Proc. AAMAS*, 2012, pp. 105–112.

[35] J. Chen *et al.*, "Decentralized data fusion and active sensing with mobile sensors for modeling and predicting spatiotemporal traffic phenomena," in *Proc. UAI*, 2012, pp. 163–173.

[36] R. Ouyang, K. H. Low, J. Chen, and P. Jaillet, "Multi-robot active sensing of non-stationary Gaussian process-based environmental phenomena," in *Proc. AAMAS*, Richland, SC, USA, 2014, pp. 573–580.

[37] R. Ouyang, K. H. Low, J. Chen, and P. Jaillet, "Gaussian process-based decentralized data fusion and active sensing for mobility-on-demand system," in *Proc. Robot. Sci. Syst.*, 2013, pp. 573–580.

[38] J. Chen, K. H. Low, Y. Yao, and P. Jaillet, "Gaussian process decentralized data fusion and active sensing for spatiotemporal traffic modeling and prediction in mobility-on-demand systems," *IEEE Trans. Autom. Sci. Eng.*, vol. 12, no. 3, pp. 901–921, Jul. 2015.

[39] K. Wang, D. Zhang, Y. Li, R. Zhang, and L. Lin, "Cost-effective active learning for deep image classification," *IEEE Trans. Circuits Syst. Video Technol.*, vol. 27, no. 12, pp. 2591–2600, Dec. 2017.

[40] J. M. Haut, M. E. Paoletti, J. Plaza, J. Li, and A. Plaza, "Active learning with convolutional neural networks for hyperspectral image classification using a new Bayesian approach," *IEEE Trans. Geosci. Remote Sens.*, vol. 56, no. 11, pp. 6440–6461, Nov. 2018.

[41] W. H. Beluch, T. Genewein, A. Nürnberger, and J. M. Köhler, "The power of ensembles for active learning in image classification," in *Proc. IEEE Conf. Comput. Vis. Pattern Recognit.*, 2018, pp. 9368–9377.

[42] J.-J. Zhu and J. Bento, "Generative adversarial active learning," 2017. [Online]. Available: arXiv:1702.07956

[43] Y. Liu *et al.*, "Generative adversarial active learning for unsupervised outlier detection," *IEEE Trans. Knowl. Data Eng.*, to be published.

[44] C. Xu and W. Tao, "Combining active learning and semi-supervised learning by using selective label spreading," in *Proc. ICDMW*, 2017, pp. 146–157.

[45] A. Krizhevsky, I. Sutskever, and G. E. Hinton, "ImageNet classification with deep convolutional neural networks," in *Proc. Adv. Neural Inf. Process. Syst.*, 2012, pp. 1106–1114.

[46] M. Montemerio, S. Thrun, D. Koller, and B. Wegbreit, "Fast-SLAM: A factored solution to simultaneous mapping and localization," in *Proc. AAAI*, 2002, pp. 593–598.

[47] K. Murphy and S. Russell, "Rao-blackwellised particle filtering for dynamic Bayesian networks," in *Sequential Monte Carlo Methods in Practice*. New York, NY, USA: Springer, 2001, pp. 499–515.

[48] D. Hahnel, W. Burgard, D. Fox, and S. Thrun, "An efficient FastSLAM algorithm for generating maps of large-scale cyclic environments from raw laser range measurements," in *Proc. IEEE Int. Conf. Robot. Autom.*, vol. 1, 2003, pp. 206–211.

[49] Y. Gal, R. Islam, and Z. Ghahramani, "Deep Bayesian active learning with image data," in *Proc. Int. Conf. Mach. Learn.*, 2017, pp. 1183–1192.

[50] C. E. Shannon, "A mathematical theory of communication," *Bell Syst. Techn. J.*, vol. 27, no. 3, pp. 379–423, 1948.

[51] D. Barber and F. V. Agakov, "The IM algorithm: A variational approach to information maximization," in *Proc. Adv. Neural Inf. Process. Syst.*, vol. 16, 2004, pp. 201–208.

[52] J.-Q. Li, W.-L. Li, G.-Q. Deng, and Z. Ming, "Continuous-behavior and discrete-time combined control for linear induction motor-based urban rail transit," *IEEE Trans. Magn.*, vol. 52, no. 7, pp. 1–4, Jul. 2016.

[53] Y. Song, L. Liu, H. Ma, and A. V. Vasilakos, "A biology-based algorithm to minimal exposure problem of wireless sensor networks," *IEEE Trans. Netw. Service Manag.*, vol. 11, no. 3, pp. 417–430, Sep. 2014.

[54] L. Liu, Y. Song, H. Zhang, H. Ma, and A. V. Vasilakos, "Physarum optimization: A biology-inspired algorithm for the Steiner tree problem in networks," *IEEE Trans. Comput.*, vol. 64, no. 3, pp. 818–831, Mar. 2015.

[55] J. Li, L. Huang, Y. Zhou, S. He, and Z. Ming, "Computation partitioning for mobile cloud computing in a big data environment," *IEEE Trans. Ind. Informat.*, vol. 13, no. 4, pp. 2009–2018, Aug. 2017.

[56] A. Ranganathan and S. Koenig, "PDRRTS: Integrating graph-based and cell-based planning," in *Proc. IEEE IROS*, vol. 3, 2004, pp. 2799–2806.

Jianqiang Li received the B.S. and Ph.D. degrees from the South China University of Technology, Guangzhou, China, in 2003 and 2008, respectively.

He is a Professor with the College of Computer and Software Engineering, Shenzhen University, Shenzhen, China. He led three projects of the National Natural Science Foundation and three projects of the Natural Science Foundation of Guangdong, China. His major research interests include robotic, hybrid systems, Internet of Things, and embedded systems.

Zhuangzhuang Chen received the B.Sc. degree from Jiangnan University, Wuxi, China, in 2016, and the M.Sc. degree in CS from Shenzhen University, Shenzhen, China, in 2019.

His current research interests include robotic, embedded systems, and machine learning methods for unsupervised and semisupervised learning in dynamic environments.

Jie Chen received the B.Sc. degree in EE from Taizhou University, Taizhou, China, in 2006, the M.Sc. degree in CS from Zhejiang University, Hangzhou, China, in 2008, and the Ph.D. degree in CS from the National University of Singapore (NUS), Singapore, in 2013.

He was a Postdoctoral Associate with Singapore-MIT Alliance for Research and Technology (SMART), Singapore. In 2018, he joined the Shenzhen University, Shenzhen, China, as a Research-Track Associate Professor. His research interests include machine learning, multiagent system, robotics, intelligent transportation system, and intelligent healthcare system.

Dr. Chen received the Dean's Graduate Research Excellence Award from NUS in 2013. He was a Program Committee Member in IJCAI, AAAI, and ICRA.

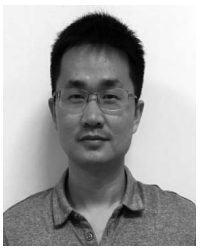

Qiuzhen Lin received the Ph.D. degree from the Department of Electronic Engineering, City University of Hong Kong, Hong Kong, in 2014.

He is currently an Associate Professor with the College of Computer Science and Software Engineering, Shenzhen University, Shenzhen, China. He has published over 40 research papers since 2008. His current research interests include the artificial immune system, multiobjective optimization, and dynamic system.